LETTERS

Fracture surface energy of the Punchbowl fault, San Andreas system

Judith S. Chester[1], Frederick M. Chester[1] & Andreas K. Kronenberg[1]

Fracture energy is a form of latent heat required to create an earthquake rupture surface and is related to parameters governing rupture propagation and processes of slip weakening[1–3]. Fracture energy has been estimated from seismological and experimental rock deformation data[4–8], yet its magnitude, mechanisms of rupture surface formation and processes leading to slip weakening are not well defined[8–10]. Here we quantify structural observations of the Punchbowl fault, a large-displacement exhumed fault[11,12] in the San Andreas fault system, and show that the energy required to create the fracture surface area in the fault is about 300 times greater than seismological estimates would predict for a single large earthquake. If fracture energy is attributed entirely to the production of fracture surfaces, then all of the fracture surface area in the Punchbowl fault could have been produced by earthquake displacements totalling <1 km. But this would only account for a small fraction of the total energy budget, and therefore additional processes probably contributed to slip weakening during earthquake rupture.

Numerous models have been proposed that provide a basis for relating the macroscopic energy budget to physical processes of earthquake slip[10,13]. In the commonly used slip-weakening model, the elastic strain energy released during an earthquake is partitioned between the fracture energy, E_G, the frictional heat, E_H, and the energy radiated as seismic waves, E_R (refs 10, 14) (Fig. 1). E_H, often considered a large component of the total energy budget, does not directly influence earthquake rupture dynamics, whereas the relative magnitude of E_R to E_G, expressed by radiation efficiency $\eta_R = E_R/(E_R + E_G)$, plays a fundamental role[2,14,15]. E_G describes the flow of energy at rupture tips that is required to form a rupture surface and produce a breakdown in strength[1,2] (Fig. 1). For small E_G ($\eta_R = 1$), an earthquake rupture is considered very brittle, rupture speed is rapid, and growth is favoured. Currently, the details of energy partitioning, the magnitude of each energy term, and whether η_R varies with earthquake magnitude and tectonic setting are not well known[13–15].

Some constraints on E_G are provided by laboratory estimates of the specific fracture energy, G, defined by $G = E_G/S$, where S is the area of the rupture surface[10]. For a tensile fracture in brittle material, G is nearly equivalent to the free-surface energy of the fracture[16,17]. Experiments show that G for shear fracture of intact rock under pressures up to 470 MPa is greater than that for tensile cracking, and that G increases with normal stress and roughness for frictional slip[4,5,18]. These observations may reflect the formation of microfractures and extreme fragmentation associated with the formation of shear surfaces[4,19–22]. Some seismologic data suggest that G increases with earthquake size[8], qualitatively consistent with scaling relations between rupture dimension and extent of associated fracture damage[22]. Yet whether other processes, such as fluid pressurization or melt lubrication, also contribute to rupture formation and the breakdown in strength is still unknown[8–10,23].

To answer this question, the magnitude of the total free-surface energy of fractures produced during an earthquake rupture must be determined. It is essential that this estimate should account for the fracture surface energy in the broad zone of damage bounding a fault, as well as that harboured within the narrow, intensely fragmented core[2,3,7]. Accordingly, we use structural observations of the Punchbowl fault zone to quantify the total fracture surface area, S_T, which includes the surface area of cataclastic particles in the ultracataclasite, S_{UC}, the surface area of gouge particles in subsidiary faults of the damage zone, S_{SF}, and the surface area of microfractures in the damage zone, S_{MF} (Fig. 2). This study provides the first quantification of fracture surface area over the entire deformed zone of a mature fault expressed as fracture surface area per unit area (in m^2) of the macroscopic fault surface. The surface area of each component is determined by direct observation of fractures and particle sizes, and scaling relations for particle size and subsidiary fault length, thickness and density. We use S_T to calculate the total fracture surface energy and relate this to the G of an earthquake. In so doing, we assume that all fracture damage in the Punchbowl fault zone was produced during seismic slip[12].

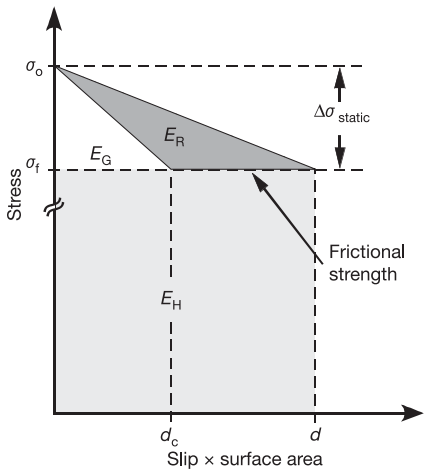

Figure 1 | Simple representation of the energy budget for earthquakes on the basis of fault slip-weakening models[10,14,15]. The upper line bounding region E_R shows a shear stress drop from initiation of earthquake slip to a total slip, d. Frictional, or resistive, strength is shown by the lower line bounding region E_R. Frictional strength decreases with slip over a characteristic displacement, d_c, to a residual friction level. For brevity, more complex variations in shear stress and resistive strength expected for actual earthquake events[13,15] are not shown. σ_o, initial stress; σ_f, final, frictional stress. Details of energy partitioning are model-specific. In general, however, the radiated energy, E_R, is the difference between the mean shear stress and mean resistive strength[2,15].

[1]Center for Tectonophysics, Department of Geology & Geophysics, Texas A&M University, College Station, Texas 77843-3115, USA.

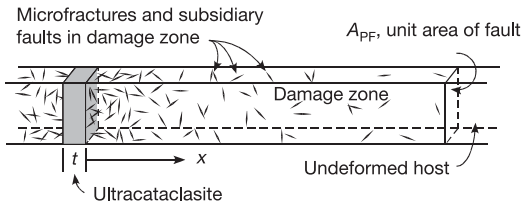

Figure 2 | Structural model of the Punchbowl fault zone for calculating fracture surface area. Domains of damaged rock containing subsidiary faults and microfractures are bounded by undeformed host rock. The central core of the fault contains an ultracataclasite layer of thickness *t*. Total fracture surface area, $S_T = S_{UC} + S_{SF} + S_{MF}$, is determined within the column of rock across the entire fault zone of cross-sectional area $A_{PF} = 1\,m^2$. Calculations assume damage is symmetric about the ultracataclasite layer.

The Punchbowl fault is a 200-m-thick zone of fractured rock containing a core several metres thick of sheared cataclasite and ultracataclasite[11,12,24]. The fault records extreme localization of slip similar to other ancient exhumed and active seismic faults[12]. The Punchbowl fault juxtaposes igneous and metamorphic rocks of the San Gabriel complex and arkosic sandstones of the Punchbowl Formation along a continuous layer of ultracataclasite. Deformation is dominantly brittle and the fault is exhumed to a depth of 2–4 km (ref. 11). The ultracataclasite layer is 4 cm to 1 m thick, and displays a relatively planar, continuous surface that served as the principal slip surface during the last several kilometres of displacement[12]. The principal slip surface is a layer 1 mm thick of ultracataclasite distinguished by uniform birefringence, contains porphyroclasts of older ultracataclasite that record reworking, and has at least one relatively distinct and planar boundary[25]. Particles greater than 10 μm in diameter constitute 28% of the ultracataclasite, the majority of which are fragments of microscopic veins[11]. Transmission electron microscopy reveals particles of host rock less than 100 nm in diameter[25] (Fig. 3). The smallest (4 to 50 nm) particles imaged are cataclastic particles or euhedral grains produced by syn- and post-faulting reaction. Measurements of particle size in plane section[12] are consistent with $N(D) = cD^{-a}$, where D is particle diameter, $N(D)$ is the number of particles for each size bin, and a and c are constants, with $a = 2.0$ and $c = 0.07$ (Fig. 3b).

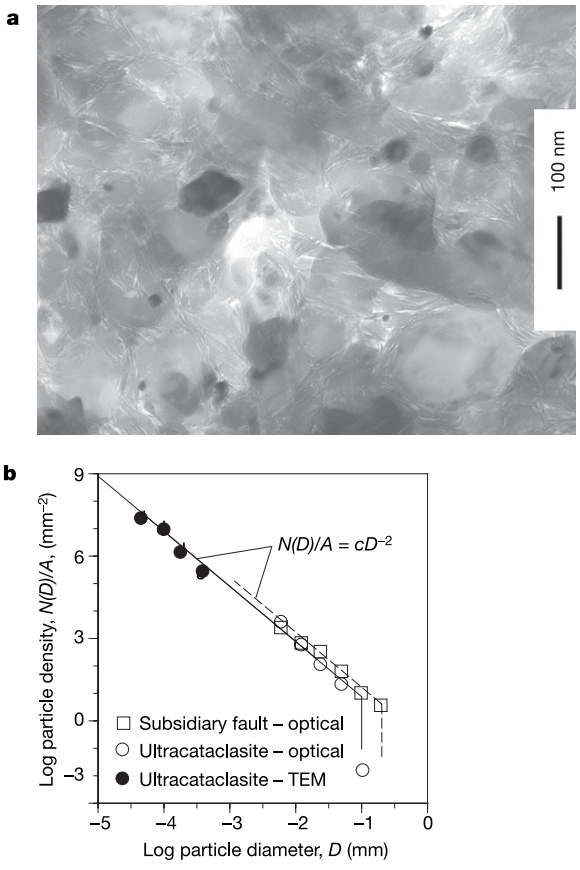

Figure 3 | Particle size of ultracataclasite and subsidiary fault cataclasite. **a**, TEM image of ultracataclasite showing particles 10 to 200 nm in diameter. **b**, Measurements of particle density as a function of particle diameter, where density is given as number of particles in a class size, $N(D)$, divided by area, A. Class sizes from 50–400 nm are imaged using TEM[25] and from 6–400 μm are imaged optically[12]. All measurements are consistent with a power-law relation with slope of −2. Solid and dashed lines show particle size distributions assumed for the fracture surface area calculations of ultracataclasite and subsidiary fault cataclasite, respectively.

The total fracture surface area in the ultracataclasite is determined assuming spherical particles with a power-law size distribution. Our observations indicate that the upper cut-off is 0.1 mm, and we assume that particles <50 nm in diameter follow the same power-law distribution to a lower cut-off of 1.6 nm. Using a mean layer thickness of 0.3 m and the ratio of surface area to volume for spheres ($3/r$), gives a S_{UC} of $1.3 \times 10^8\,m^2$ per unit area of the fault surface. The total surface area in the 1-mm-thick principal slip surface is $4.2 \times 10^5\,m^2$ per unit area. The surface area per unit volume of the Punchbowl ultracataclasite is similar to that determined for gouge of the San Andreas fault at Tejon Pass[26].

Subsidiary faults of the damage zone are consistent with scaling relations between number, length, displacement and thickness of brittle faults in crustal rock[22,27]. Faults typically are metres in length, <1 mm thick and display centimetre offsets. Faults up to 1–2 cm thick, with 1–2-m offsets, are also present[11] (Fig. 4). Linear density, P_L, of subsidiary faults in the Punchbowl Formation decreases with the logarithm of distance from the ultracataclasite (Fig. 4). For the entire damage zone, we assume $N(L) = cL^{-a}$, where L is fault length, $N(L)$ is the number of faults for each length bin, $a = 1$ and $c = 2{,}500$, the ratio of fault displacement to length is 0.01, and the ratio of thickness to displacement is 0.005.

Subsidiary fault gouge is coarser-grained than the ultracataclasite (Fig. 3b), and particles 100–200 μm in diameter comprise 25% of the total volume. We assume particle size distributions fit $N(D) = cD^{-a}$ with constants $a = 2.0$ and $c = 0.15$, and have an upper cut-off of 200 μm and lower cut-off of 0.8 μm. Assuming the orientation of subsidiary faults is isotropic, such that the surface area is twice P_L (ref. 28), integrating over the damage zone, and using scaling relations for fault thickness and particle size, we calculate a value for S_{SF} of $3.3 \times 10^6\,m^2$ per unit area of the fault surface.

The linear density of microfractures in the Punchbowl Formation decreases with the logarithm of distance from the ultracataclasite to a constant, regional density at approximately 100 m (Fig. 4). Integrating over the damage zone, assuming microfracture orientations are isotropic, and doubling for the two surfaces of a microfracture, gives a value for S_{MF} of $2.4 \times 10^6\,m^2$ per unit fault area.

The total fracture surface area in the damage zone ($S_{SF} + S_{MF}$) is less than 10% of that in the ultracataclasite layer, giving a total fracture surface area for the entire fault zone, S_T, of $1.4 \times 10^8\,m^2$ per unit fault area. Assuming the free-surface energy to be $1\,J\,m^{-2}$, and that the geometric surface area should be increased by about a factor of five to account for non-spherical grain shapes and finer-scale roughness[16,19,26], brings the total fracture surface energy to $7 \times 10^8\,J$ per unit fault area. Fracture surface energy of the millimetres-thick principal slip surface is $2 \times 10^6\,J$ per unit area of the fault surface.

To estimate the energy required to create fracture surfaces during a single earthquake, we divide the total energy by 10,000 large earthquakes (to account for 44 km of total displacement), which yields $7 \times 10^4\,J\,m^{-2}$ per earthquake. This estimate is a lower bound because it does not include the energy associated with refracturing healed grain boundaries and comminuted grains enlarged by Ostwald

ripening. As an example, if 50% of the ultracataclasite in the millimetres-thick principal slip surface was refractured during an earthquake, and the energy to refracture a grain boundary is half of that required to fracture an intact grain, then fracture surface energy for a single earthquake increases to approximately $5 \times 10^5\,J\,m^{-2}$.

Our estimate of the energy required to create fracture surfaces during a single earthquake is small (<1%) relative to estimates of E_H/S for the Punchbowl fault at a depth of 2–4 km, which even for a coefficient of friction of 0.2 is about $5 \times 10^7\,J\,m^{-2}$. This is in direct contrast to a recent conclusion that the surface energy of gouge constitutes half or more of the earthquake energy budget[26]. Our estimate also cannot account for seismologic values of G (about $10^6\,J\,m^{-2}$; refs 6–8) unless we assume that a significant number of healed grain boundaries and ripened grains are refractured in each successive earthquake, and that all fracturing is attributed to the breakdown phase of rupture. Because some proportion of fracture surface area must be produced during sliding at residual friction[21], additional processes such as lubrication, flash heating, and thermal pressurization probably contribute to the breakdown in strength[8–10,23]. These latter processes are compatible with the microstructure of the Punchbowl fault ultracataclasite[12,25,29], but would not be recorded by fracture surface area.

The total cumulative fracture surface energy of the Punchbowl fault is about 300 times greater than the fracture energy, G, for a single large earthquake. If G is attributed entirely to the creation of fracture surface, then the observed damage could be produced by earthquake slip totalling less than 1 km of displacement. The different estimates of fracture surface area created during seismic slip on a mature fault versus that associated with mining-induced ruptures[19,20,26] may be explained by extensive fracturing during fault formation and less fracturing associated with slip on an established fault surface. This explanation is consistent with large values of G determined in the laboratory for shear fracture relative to that for frictional sliding[4,5]. Our results are also consistent with previous conclusions that the overall structure of large-displacement faults is established early in faulting history[12,30].

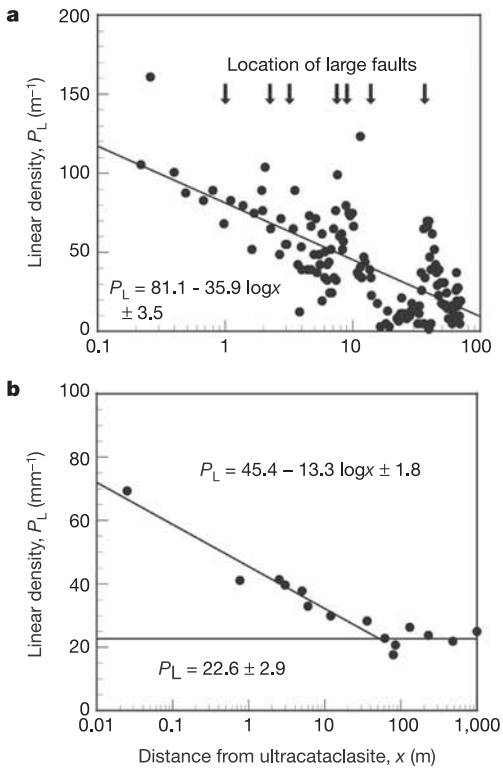

Figure 4 | Subsidiary fault and microfracture density in the damaged Punchbowl Formation along the fault[24]. Solid line shows best-fit relations (with 95% confidence interval) assumed for calculating fracture surface area. **a**, Linear density of subsidiary faults measured along four traverses across the damage zone (solid circles). Locations of subsidiary faults of the largest size class (gouge layers 1–2 cm thick) are identified with arrows. **b**, Linear density of microfractures (solid circles). At distances greater than approximately 100 m, microfracture density reflects regional density. The difference between near-fault and regional distributions is used to calculate the fracture surface area associated with faulting.

Received 9 January; accepted 15 June 2005.

1. Ida, Y. Cohesive force across the tip of a longitudinal-shear crack and Griffith's specific surface energy. *J. Geophys. Res.* **77,** 3796–3805 (1972).
2. Husseini, M. I. & Randall, M. J. Rupture velocity and radiation efficiency. *Bull. Seismol. Soc. Am.* **66,** 1173–1187 (1976).
3. Andrews, D. J. Rupture dynamics with energy loss outside the slip zone. *J. Geophys. Res.* **110,** B01307 (2005).
4. Wong, T. F. Shear fracture energy of Westerly granite from post-failure behaviour. *J. Geophys. Res.* **87,** 990–1000 (1982).
5. Okubo, P. G. & Dieterich, J. H. Effects of physical fault properties on frictional instabilities produced on simulated faults. *J. Geophys. Res.* **89,** 5817–5827 (1984).
6. Guatteri, M., Spudich, P. & Beroza, G. C. Inferring rate and state friction parameters from a rupture model of the 1995 Hyogo-ken Nanbu (Kobe) Japan earthquake. *J. Geophys. Res.* **106,** 26511–26521 (2001).
7. Rice, J. R., Sammis, C. G. & Parsons, R. Off-fault secondary failure induced by a dynamic slip-pulse. *Bull. Seismol. Soc. Am.* **95,** 109–134 (2005).
8. Abercrombie, R. E. & Rice, J. R. Can observations of earthquake scaling constrain slip weakening? *Geophys. J. Int.* **162,** 406 (2005).
9. Heaton, T. H. Evidence for and implications of self-healing pulses of slip in earthquake rupture. *Phys. Earth Planet. Inter.* **64,** 1–20 (1990).
10. Kanamori, H. & Heaton, T. H. in *GeoComplexity and the Physics of Earthquakes* (eds Rundle, J. B., Turcotte, D. L. & Klein, W.) (American Geophysical Union, Washington DC, 2000).
11. Chester, F. M. & Logan, J. M. Composite planar fabric of gouge from the Punchbowl fault, California. *J. Struct. Geol.* **9,** 621–634 (1987).
12. Chester, F. M., Chester, J. S., Kirschner, D. L., Schulz, S. E. & Evans, J. P. in *Rheology and Deformation in the Lithosphere at Continental Margins* (eds Karner, G. D., Taylor, B., Driscoll, N. W. & Kohlstedt, D. L.) (Columbia Univ. Press, New York, 2004).
13. Kanamori, H. Mechanics of earthquakes. *Annu. Rev. Earth Planet. Sci.* **22,** 207–237 (1994).
14. Venkataraman, A. & Kanamori, H. Observational constraints on the fracture energy of subduction zone earthquakes. *J. Geophys. Res.* **109,** B05302 (2004).
15. Beeler, N. M., Wong, T. F. & Hickman, S. H. On the expected relationships among apparent stress, static stress drop, effective shear fracture energy, and efficiency. *Bull. Seismol. Soc. Am.* **93,** 1381–1389 (2003).
16. Brace, W. F. & Walsh, J. B. Some direct measurements of the surface energy of quartz and orthoclase. *Am. Mineral.* **47,** 1111–1122 (1962).
17. Friedman, M., Handin, J. & Alani, G. Fracture-surface energy of rocks. *Int. J. Rock Mech. Mining Sci.* **9,** 757–766 (1972).
18. Wong, T. F. in *Earthquake Source Mechanics* (eds Das, S., Boatwright, J. & Scholz, C. H.) 1–12 (American Geophysical Union, Washington DC, 1986).
19. Olgaard, D. L. & Brace, W. F. The microstructure of gouge from a mining-induced seismic shear zone. *Int. J. Rock Mech. Mining Sci.* **20,** 11–19 (1983).
20. McGarr, A., Spottiswoode, S. M., Gay, N. C. & Ortlepp, W. D. Observations relevant to seismic driving stress, stress drop, and efficiency. *J. Geophys. Res.* **84,** 2251–2261 (1979).
21. Yund, R. A., Blanpied, M. L., Tullis, T. E. & Weeks, J. D. Amorphous material in high strain experimental fault gouges. *J. Geophys. Res.* **95,** 15589–15602 (1990).
22. Scholz, C. H., Dawers, N. H., Yu, J. Z., Anders, M. H. & Cowie, P. A. Fault growth and fault scaling laws: Preliminary results. *J. Geophys. Res.* **98,** 21951–21961 (1993).
23. Andrews, D. J. A fault constitutive relation accounting for thermal pressurization of pore fluid. *J. Geophys. Res.* **107,** ESE15-1–8, art. no. 2363 (2002).
24. Wilson, J. E., Chester, J. S. & Chester, F. M. Microfracture analysis of fault growth and wear processes, Punchbowl Fault, San Andreas System, California. *J. Struct. Geol.* **25,** 1855–1873 (2003).
25. Chester, J. S., Kronenberg, A. K., Chester, F. M. & Guillemette, R. N. Characterization of natural slip surfaces relevant to earthquake mechanics. *Eos* **84**(46) (2003).
26. Wilson, B., Dewers, T., Reches, Z. & Brune, J. Particle size and energetics of gouge from earthquake rupture zones. *Nature* **434,** 749–752 (2005).
27. Bonnet, E. *et al.* Scaling of fracture systems in geological media. *Rev. Geophys.* **39,** 347–383 (2001).

28. Underwood, E. E. *Quantitative Stereology* (Addison Wesley, Reading, Massachusetts, 1970).
29. Sibson, R. H. Thickness of the seismic slip zone. *Bull. Seismol. Soc. Am.* **93**, 1169–1178 (2003).
30. Evans, J. P., Shipton, Z. K., Pachell, M. A., Lim, S. J. & Robeson, K. in *Proc. 3rd Conf. on Tectonic Problems of the San Andreas Fault System* (eds Bokelmann, G. & Kovach, R. L.) 67–81 (Stanford Univ. Publ., 2000).

Acknowledgements We thank P. Spudich , T. Heaton and N. Beeler for discussions and review of an early version of this paper, and J. Jenson for advice regarding data analysis. The TEM work was performed in the Microscopy and Imaging Center of Texas A&M University and Z. Luo is acknowledged for his assistance. This research was supported by the Southern California Earthquake Center through a NSF and USGS Cooperative Agreement (J.S.C.), US National Science Foundation (J.S.C. and F.M.C.), and US Geological Survey (J.S.C.).

Author Information Reprints and permissions information is available at npg.nature.com/reprintsandpermissions. The authors declare no competing financial interests. Correspondence and requests for materials should be addressed to J.S.C. (chesterj@geo.tamu.edu).